

Cross Vapor Stream Effect on Falling Film Evaporation in Horizontal Tube Bundle Using R134a

Chuang-Yao Zhao, Wen-Tao Ji, Pu-Hang Jin & Wen-Quan Tao

To cite this article: Chuang-Yao Zhao, Wen-Tao Ji, Pu-Hang Jin & Wen-Quan Tao (2017): Cross Vapor Stream Effect on Falling Film Evaporation in Horizontal Tube Bundle Using R134a, Heat Transfer Engineering, DOI: [10.1080/01457632.2017.1327296](https://doi.org/10.1080/01457632.2017.1327296)

To link to this article: <https://doi.org/10.1080/01457632.2017.1327296>



Accepted author version posted online: 22 May 2017.
Published online: 13 Jul 2017.



[Submit your article to this journal](#) 



Article views: 45



[View related articles](#) 



[View Crossmark data](#) 



Citing articles: 3 [View citing articles](#) 



Cross Vapor Stream Effect on Falling Film Evaporation in Horizontal Tube Bundle Using R134a

Chuang-Yao Zhao, Wen-Tao Ji, Pu-Hang Jin, and Wen-Quan Tao

Key Laboratory of Thermo-Fluid Science and Engineering, School of Energy and Power Engineering, Xi'an Jiaotong University, Xi'an, China

ABSTRACT

The falling film evaporation of R134a with nucleate boiling outside a triangular-pitch (2-3-2-3) tube bundle is experimentally investigated, and the effects of saturation temperature, film flow rate and heat flux on heat transfer performance are studied. To study the effect of cross vapor stream on the falling film evaporation, a novel test section is designed, including the tube bundle, liquid and extra vapor distributors. The measurements without extra vapor are conducted at the saturation temperature of 6, 10 and 16°C, film Reynolds number of 220 to 2650, and heat flux of 20 to 60 kWm⁻². Cross vapor stream effect experiments are operated at three heat fluxes 20, 30, and 40 kWm⁻² and two film flow rates of 0.035 and 0.07 kgm⁻¹s⁻¹, and the vapor velocity at the smallest clearance in the tube bundle varies from 0 to 2.4 ms⁻¹. The results indicate that: film flow rate, heat flux and saturation temperature significantly influence the heat transfer; the cross vapor stream either promote or inhibit the falling film evaporation, depending on the tube position, film flow rate, heat flux and vapor velocity.

Introduction

In recent years, the application of falling film evaporation outside the horizontal tube has attracted great attentions in the large refrigeration and air-conditioning systems. Many investigations have indicated that this technology is a potential alternative to the flooded evaporation due to superiorities of less refrigerant charge, higher heat transfer coefficient, easier lubrication return, and negligible static pressure difference etc. However, the design of falling film evaporation is extremely complicated because of many influencing factors, among which the vapor stream effect is one of the most important one.

In the operation of a falling film evaporator with large tube bundle the liquid film is considerably troubled by the massive vapor stream, which probably cause liquid film redistribution and even induce film breakout. All of these influences will eventually result in the fluctuation of the heat transfer performance. Up to days, there is yet no clear understanding on the influencing of vapor stream on the falling film heat transfer, harmful or beneficial. In general, the random direction of the vapor flow in the tube bundle can be simplified into three cases: countercurrent (upward), concurrent (downward) or crosscurrent (sideward).

In recent decade, several comprehensive reviews are conducted in [1–3], from which we can learn that the previous studies have focused on how the film flow rate, heat flux [4], operation temperature [5, 6] tube/bundle geometries [7, 8], and liquid distributor [9] affect the falling film heat transfer. A summary of the published researches on the vapor/air stream effects on falling film evaporation are listed in Table 1 [10–18]. According to these studies, the effects of the vapor/air stream on falling film heat transfer are classified into three categories. (1) Positive effects, such as Parken [10] found that the concurrent air enhances the heat transfer despite suppression in bubble nucleation with increase of vapor velocity from 9.0 to 18.0 ms⁻¹, which is attributed to the reduction in film thickness and increasing in liquid film velocity; Armbruster and Mitrovic [11] found that the sub-cooled water film heat transfer is significantly enhanced by countercurrent wet air flow at smaller air velocity, and the enhancement is highly dependent on the humidity of the air; Hu [12] also reported that the convective heat transfer is enhanced by the concurrent air flow when air velocity is up to 15 ms⁻¹; Tatara and Payvar [13] found that the falling film heat transfer of tube bundle are promoted by the countercurrent vapor flow. (2) Negative

Table 1. The studies on the effects of vapor/air flow on falling film evaporation outside horizontal tubes.

	Vapor flow direction	Liquid/gas	Bundle geometries	Comments
[10]	Concurrent	Water/air	Single tube	Boiling
[11]	Counter-current	Water/air	Single tube	Noboiling
[12]	Concurrent	Water, 41.6% ethyl alcohol and 58.4% water/air	1 × 2 bundle	Noboiling
[13]	Counter-current	R11/vapor	Triangular	Boiling
[14]	Concurrent, counter-current	Water/air	Single tube	Boiling
[15]	Concurrent, counter-current	R134a/vapor	6 to 10 tubes	Boiling
[16]	Counter-current	R134a/vapor	1 × 8 bundle	Boiling
[17]	Counter-current	R113/vapor	Triangular, diamond	Boiling
[18]	Counter-current	Water, ethylene glycol/air	1 × 3 bundle	Adiabatic

effects, such as Liu [14] found that counter-current air flow is unfavorable to heat transfer because of increasing in film thickness by the adverse shearing; Ribatski and Thome [15] found that the counter-current vapor dramatically enlarges the dry area and deteriorates heat transfer except the top tube; (3) Negligible effect, Liu [14] did not find remarkable influence of concurrent vapor flow, and Ribatski and Thome [15] found that concurrent vapor had no effect on both film flow and heat transfer. More recently, Ji et al. [16] tested the counter-current vapor stream on the falling film boiling of R134a in a tube bundle and found that the vapor generally has little effect on heat transfer when vapor velocity less than 0.5 ms^{-1} .

The behaviors of vapor stream effects are complicated, depending on the bundle arrangements, bundle depth, heat flux, film flow rate, and the level of vapor velocity. Ribatski and Thome [15] observed that the counter-current vapor flow holds up the film and so cut off the continuity liquid flow from up to down. Danilova et al. [17] thought that the counter-current vapor flow either stagnates or accelerates the liquid film flow depending on the vapor velocity. Ruan et al. [18] found that the liquid film will become unsteady when the counter-current air velocity is larger than 3.5 ms^{-1} .

For adiabatic condition, Yung et al. [19] analyzed the effects of cross vapor stream on the flow patterns transition. They predicated the critical film flow rate beyond which the flow pattern would transit from droplet to column:

$$\Gamma_{trans} = 0.81 \frac{\rho_L \pi d_p}{\lambda_t} (2\pi \sigma / \rho_L \lambda_t^3)^{1/2} \quad (1)$$

where ρ_L is liquid density, σ is surface tension, $\lambda = 2\pi (n\sigma / \rho_L g)^{0.5}$ is the wavelength of Taylor instability wave with $n = 2$ for thin liquid film and $n = 3$ for thick liquid

Table 2. The test parameters covered in this paper.

Case	Without extra vapor	With extra vapor
Refrigerant	R134a	
Saturation temperature, °C	6, 10, 16	6
Film Reynolds number	220 ~ 2650	560, 1120
Heat flux, kWm^{-2}	20, 40, 60	20, 30, 40
Vapor velocity, ms^{-1}	0	0–2.4

film, $d_p = 3(\sigma / \rho_L g)^{0.5}$ is the largest droplet diameter. At a given liquid flow rate and tube pitch, they derived the maximum allowable velocity beyond which the droplet would deflect from the below tube:

$$u_G = \left(3 \frac{\rho_L}{\rho_G} dg \tan \theta \right)^{1/2} \quad (2)$$

and the critical allowable velocity beyond which the column would not impinge onto the below tube:

$$u_G = \left(\frac{\tan \theta}{\cos \theta} \frac{4\lambda_t \Gamma g}{d^* \rho_G (2gS)^{1/2}} \right)^{1/2} \quad (3)$$

In equations (2) and (3), ρ_G is vapor density, $\tan \theta = 0.5[H/D_o(H/D_o - 1)]^{0.5}$ with H the tube pitch and D_o the external tube diameter, d is the droplet diameter and $d^* = (8\lambda\Gamma/\pi\rho_L)^{0.5}(2gS)^{-0.25}$ with S the net tube spacing of the liquid column.

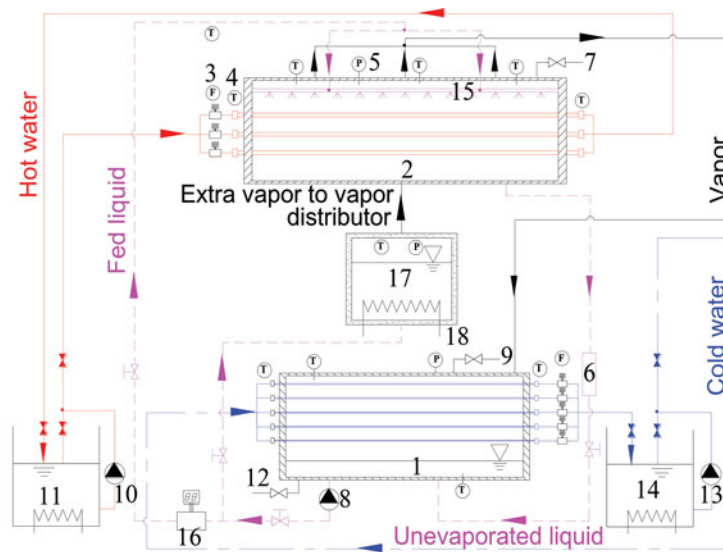
As indicated above, the effects of cross vapor stream on the falling film heat transfer in a horizontal tube bundle has yet to be reported in the literature according to the author's knowledge. The overall motivation of the present work is to quantitatively investigate the effect of vapor stream and provide some database. The major attention is focused primarily on the effect of cross vapor stream on falling film evaporation outside a horizontal tube bundle with triangular-pitch (2-3-2-3). In the experiments, the liquid is sprayed onto the tube bundle and the vapor is blown into the tube bundle from the cross direction. Tests are conducted under different film flow rates, heat fluxes, saturation temperatures, and vapor velocities. The test conditions are listed in Table 2.

In the rest sections, after a statement of the experimental setup the test procedure and data reduction method are described in order. Then the test results are demonstrated, and several conclusions are summarized finally.

Experimental setup

Test facility

Figure 1 shows the schematic diagrams of the flow loops in this test facility: refrigerant, hot water, and cold water loops.



(1) Condenser and refrigerant storage tank; (2) Falling film evaporator; (3) Electromagnetic flow meter; (4) Thermal meter; (5) Pressure gauge; (6) Condensate measuring container; (7) Exhausting valve; (8) Canned motor pump; (9) Refrigerant charging valve; (10) Hot water pump; (11) Hot water tank; (12) Refrigerant outlet; (13) Cold water pump; (14) Cold water tank; (15) Liquid distributor; (16) Coriolis mass flow meter; (17) Extra vapor generator (later added) (18) Electric heater

Figure 1. Schematic diagram of test apparatus.

During experiments, the liquid refrigerant is pumped by a canned motor pump from the bottom of the condenser (liquid tank) and then is divided into two branches. One branch is led into the boiler (vapor generator), where the refrigerant is heated and turns into vapor. This vapor serves as extra vapor flowing through the test section and then collects at the top exit and finally flows into the condenser. The other branch flows through the liquid distributor and then falls through the test section by the gravity, where the liquid refrigerant evaporates. And then the vaporized refrigerant also collects at the top exit and finally flows into the condenser, while the un-evaporated liquid collects at the bottom of the evaporator and then returns to the condenser through the link pipe. In the condenser, the condensing tubes are fixed in the condenser to condense the vapor into liquid. Hereto, the refrigerant finishes a circulation. The overall flow rate of the liquid can be adjusted by a frequency converter.

The evaporator is a stainless steel cylinder vessel with internal diameter of 450 mm and a length of 1450 mm, in which the evaporating tube bundle is going through the flanges at two ends of the evaporator, and the tubes are fixed on the flanges by expansion method. The condenser is another stainless steel cylinder vessel with internal diameter of 450 mm and a length of 1140 mm. During run, the hot and cold water pumped by their own centrifugal pumps, and flows through the evaporating and condensing tubes, and then returns to their own tanks,

respectively. The temperatures of the water in hot and cold water tank are adjusted to the required levels by using the heating and cooling devices. The overall flow rates of hot and cold water can also be adjusted by their own frequency converters and bypasses, and the flow rate of each test tube can be controlled using its own valve. The boiler is equipped with electric bars to generate vapor. The vapor velocity is determined by the saturated vapor flow rate \dot{m}_g , and the film flow rate is adjusted by the heating power P , viz. $\dot{m}_g = P/r$ with r being the latent heat. During operation, the heating power can range from 0 – 40 kW. The heating power is monitored by a dynamometer with the accuracy of 0.1 W.

The pressure of the system is measured by two pressure gauges (KELLER LEX1) with a range from -0.1 to 2.0 MPa and an accuracy of 0.05% of full scale, which locates at the top and bottom of the test section. The temperatures of the liquid and vapor refrigerant are measured by the platinum temperature transducers (Pt100) with a precision of $\pm(0.15 \pm 0.002|T|)$ K, respectively. The temperatures of the hot water at the inlet and outlet of the test tubes are measured respectively by the ultra-precise RTD (OMEGA Pt100 1/10 DIN) with an accuracy of $(0.03 + 0.0005|T|)$ K within the temperature range of this study. The flow meters of each test tube are measured by the electromagnetic flow meters (SIEMENS MAGFLO MAG5100W) with an accuracy of 0.1% of full scale, respectively. And the flow rate of the refrigerant can be

obtained by using a Coriolis mass flow meter (SIEMENS MASS2100) with an accuracy of 0.1% of full scale. All of the electric resistances of thermal transducers are measured by Keithley2700 digital voltmeter.

Test section

For this study, a novel test section is constructed based on the foregoing test facility. The special test section includes liquid distributor, vapor distributor and tube bundle, as depicted in Figure 2(a) and (b).

The liquid distributor is mainly composed of two parts: the preliminary and secondary distributors, as seen in Figure 2(b) and (c). During run, the refrigerant is firstly pumped into the preliminary distributor, which is a closed rectangular box made of stainless steel and four rows of orifices with a diameter of 2.0 mm and a row spacing of 20.0 mm (center to center) are drilled on the bottom of the box. And then, the refrigerant flows into the secondary distributor. The secondary distributor is another rectangular stainless steel box but has an opening top surface. Similarly, four rows of orifices are fabricated on the bottom. In the secondary distributor, the refrigerant flows out under the application of gravitational head. To get an optimum design, some preliminary tests using water are conducted to determine the diameter

and pitch of these orifices. According to the tests, we selected the diameter of 2.0 mm and pitch of 15.0 mm. It should note that the practical film flow rate should be within the limited one to avoid overflow in the secondary distributor.

The main body of the vapor distributor is a circular pipe with a row of orifices with a diameter of 2.0 mm and a pitch of 15.0 mm, see Figure 2(c) and (d). The vapor flows out from these orifices and via two columns of bars and three columns of tubes. The tubes are arranged with the same geometries of the test tube bundle. And finally, the vapor flows through the test tube bundle. So, the vapor experiences three times of distribution: the first for horizontal and the second and third for vertical direction. During experiments, to avoid the vapor bypassing through the liquid drain passage, a liquid container is set at the bottom of the test section, where it forms liquid a seal.

The square test section has a length of 535 mm, height of 68 mm and width of 220 mm, which contains ten tubes arranged as 2-3-2-3 triangular-pitch. The tube bundle has a longitudinal pitch of 22.5 mm and the transverse pitch of 19.9 mm (center to center). Considering the capability of the condenser, the liquid is sprayed onto four columns of tubes but only six tubes in the outer three columns serve as test tubes, and the tube labels are shown in

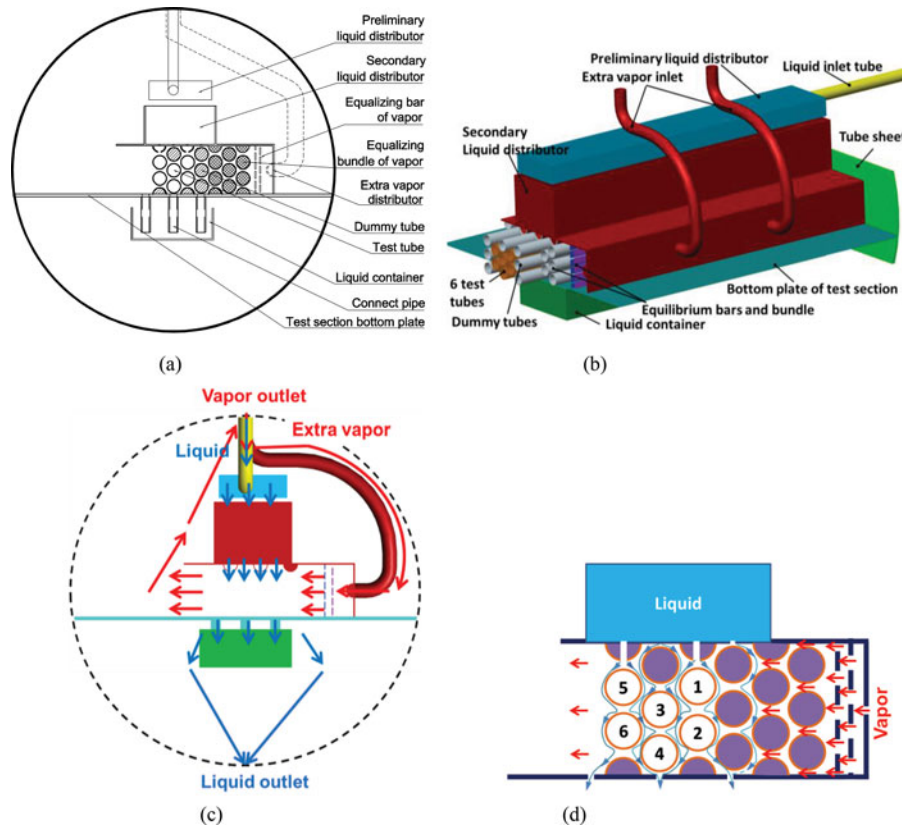


Figure 2. (a) Cross-section of test section (b) 3-d view of test section (c) Flow paths of liquid and vapor (d) tube bundle arrangement and tube label.

Figure 2(d). The test tubes are made of copper with an external fin density of 45 fpi (fins per inch), fin height of 0.535 mm and outside diameter of 19.05 mm, which is originally designed in enhancing pool boiling.

Experimental procedure

After the test section is assembled in the evaporator, the examination to verify the tightness integrity of the system is firstly conducted. For this purpose, high-pressure nitrogen is charged into the system till the internal pressure reached 1.3 MPa. Once no leak has been found, the system with pressure will be kept 72 hours and the pressure change should be less than 1000 Pa. If so, the high pressure nitrogen is discharged, and then the system is evacuated to the absolute pressure less than 800 Pa. Then the refrigerant is charged into the system through the valve. During this operation, a small amount of refrigerant is firstly charged and then evacuated by the vacuum to the above pressure level. To reduce the content of the non-condensable gases to a negligible level, this operation is repeated four times. After all preparing work completed, the refrigerant is charged into the system.

During experiments, the temperature difference between the liquid refrigerant in the tank and the one corresponding to the measured pressure according to the thermodynamics table [20] should be within ± 0.02 K, otherwise the vapor refrigerant is exhausted by the valves to eliminate non-condensable gases till it meets this criterion. This is reasonable, which has been described in [21].

Before each group of tests, the system is firstly adjusted to an equilibrium state. And the tests under one constant heat flux are accomplished within one day. The only changed parameter in one group tests is film flow rate. The equilibrium condition is identified by the difference between the saturation temperature measured by RTD and the one obtained from REFPROP [20] corresponding to the saturation pressure measured by the pressure gauges, which should be within ± 0.02 K.

Data reduction

As an isolated system, the heat balance of the experiments should be met. For the system, the hot water and the refrigerant pump (the pump needs cooling during running using the refrigerant of the system) carries energy into the system; simultaneously, the cold water carries energy away from the system, and the heat lost in the surrounding can be neglected because of good heat insulation, hence, the heat balance can be expressed as:

$$\left(\sum_{m=1}^j \Phi_{e,m} + \Phi_p - \sum_{n=1}^l \Phi_{c,n} \right) / \Phi \leq 5\% \quad (4)$$

where Φ_e and Φ_c are the input and output energy, respectively, which are determined by:

$$\Phi_{e,m} = \dot{m}_{e,m} c_{p,m} (T_{e,m,in} - T_{e,m,out}) \quad (5)$$

$$\Phi_{c,n} = \dot{m}_{c,n} c_{p,n} (T_{c,n,out} - T_{c,n,in}) \quad (6)$$

In equations (5) and (6), $T_{e,m,in}$ and $T_{e,m,out}$ denote the temperatures of inlet and outlet hot water (K) (m is the label of the test tube), respectively; $T_{c,n,in}$ and $T_{c,n,out}$ denote the temperatures of inlet and outlet cooling water via each cooling tubes (K) (n is the label of the condensing tube), respectively; $\dot{m}_{e,m}$ and $\dot{m}_{c,n}$ represent the mass flow rates of each individual heating and cooling tube ($\text{kgs}^{-1}\text{m}^{-1}$), and c_p is the specific heat capacity ($\text{Jkg}^{-1}\text{K}^{-1}$) of water based on the mean temperature of inlet and outlet water, which is obtained from the reference [22]. In addition, Φ_p is the heating power of the refrigerant pump. The reference Φ is heat transfer rate, designated as:

$$\Phi = 0.5 \left(\sum_{m=1}^j \Phi_{e,m} + \sum_{n=1}^l \Phi_{c,n} + \Phi_p \right) \quad (7)$$

In general, the overall heat transfer coefficient of each test tube is described as:

$$k_m = \frac{\Phi_{e,m}}{A_{o,m} \Delta T_{LMTD,m}} \quad (8)$$

where, A_o is the outer area of the test tube, and ΔT_{LMTD} is the logarithmic mean temperature difference, defined as:

$$\Delta T_{LMTD,m} = \frac{T_{e,m,in} - T_{e,m,out}}{\ln((T_{sat} - T_{e,m,out}) / (T_{sat} - T_{e,m,in}))} \quad (9)$$

where, T_{sat} is the saturation temperature.

For thermal resistance analysis, equation (8) is rearranged as:

$$\frac{1}{k_m} = \frac{1}{h_{i,m}} \frac{D_{o,m}}{D_{i,m}} + \frac{1}{h_{o,m}} + R_{w,m} + R_{f,m} \quad (10)$$

where D_o and D_i are the outside and inside tube diameter of the test tube. R_f is fouling thermal resistance, which was neglected because the test tubes are enough clean, and the hot water is neat enough and the test is completed soon. R_w is thermal resistance of the wall. h_i is inside convection heat transfer coefficient, which is derived from the Gnielinski equations [23], h_{gni} , multiplied by the enhancement factor c_i considering the effect of the enhanced structure of the internal surface, namely $h_i = c_i \cdot h_{gni}$. During test, the enhancement factors of all test tubes were determined by Wilson plot method. The falling film heat transfer coefficient, h_o , is thus obtained from equation (10).

The film Reynolds number of film flow is determined by:

$$Re = \frac{4\Gamma}{\mu} \quad (11)$$

where, Γ ($\text{kgm}^{-1}\text{s}^{-1}$) is the film flow rate on a single side of the test tube per unit length.

Results and discussion

Experimental uncertainty analysis

In this section, the uncertainty analysis of experimental data and the reduced results is performed. The calculation method used in this analysis is detailed in [24, 25]. Here, the uncertainties of overall and local falling film heat transfer coefficients, k and h_o are estimated. The uncertainties of k for all data are less than 3.3%. And the uncertainties of h_o vary from 19.8 to 30.9% for all experimental conditions.

Reliability validation of experimental system

A test of film condensation outside the smooth copper tube was firstly conducted in this apparatus. Then the reliability is validated by comparison between the present results and the Nusselt analytical solution [26], as displayed in Figure 3. All deviations are within 10%, from which we can say the experimental results are reliable.

The enhanced factor of the internal surface of test tubes

Wilson plot method is implemented to get the enhanced factor of the internal surface of each test tube. The tests

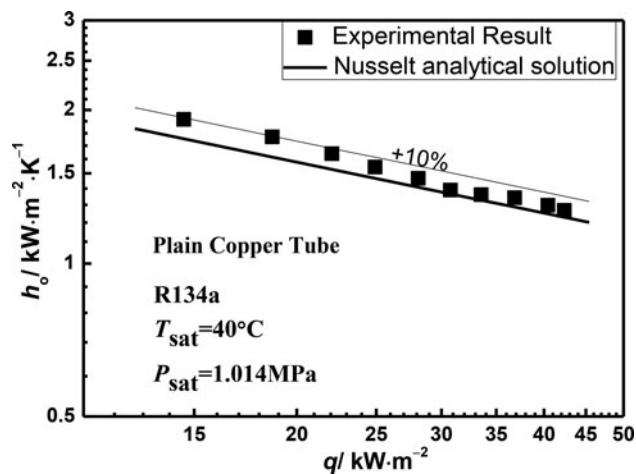


Figure 3. Comparison between the film condensing experiment results with Nusselt analytical solution [26].

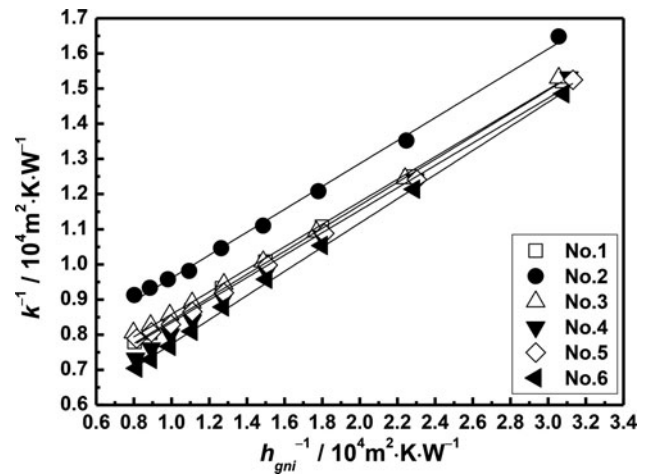


Figure 4. Wilson plots of six test tubes.

are conducted with the internal water velocity of $0.8 - 3.5 \text{ ms}^{-1}$ and nominal heat flux of 40 kWm^{-2} . Figure 4 depicts the Wilson plots of the six tested tubes. Accordingly, the enhancement factors are 3.41, 3.45, 3.49, 3.24, 3.49, and 3.25 for all tubes, respectively. Since the tubes are manufactured with the same machine and period, so the mean number, 3.39, is taken as the enhanced ratio of all test tubes.

Falling film heat transfer results without extra cross vapor stream effect

The experiments under none-effect of extra vapor stream are conducted at three saturation temperatures of 6, 10 and 16°C and three heat fluxes of 20, 40, and 60 kWm^{-2} . The measurements are carried out from higher film flow rate to the lower one.

Figures 5 to 7 show the local heat transfer coefficients varying against the film Reynolds number. It should be noted that the vapor exit is at one side of the tube bundle, so the shearing of the generated vapor still has influence on the film flow and heat transfer. From these figures, the following features can be summarized:

- (1) For all three heat fluxes and three saturation temperatures, a general trend can be seen that with decrease of film flow rate, the local heat transfer coefficient of each individual tube firstly remains constant and then declines rapidly, which is resulted from a fact that the tubes are well wetted by the liquid at larger film flow rates while partial dryout occurs at smaller film flow rates.
- (2) The transition film flow rate responsible for the onset of heat transfer decline varies with tube position and heat flux. Generally, the lower tubes have larger transition film flow rate, because these tubes encounter the film dryout much earlier.

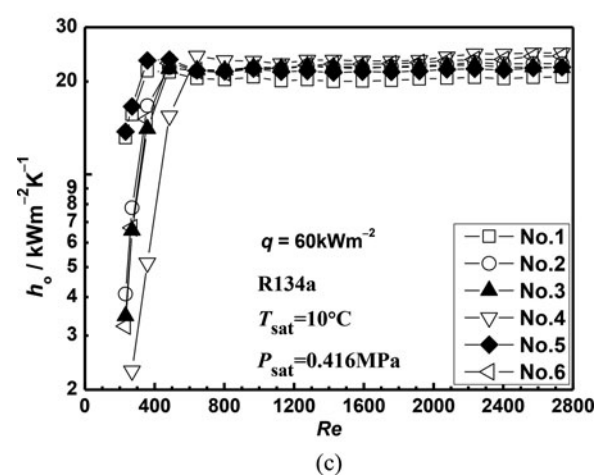
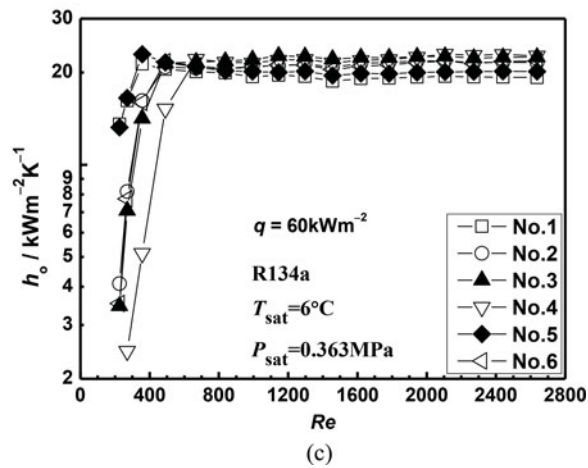
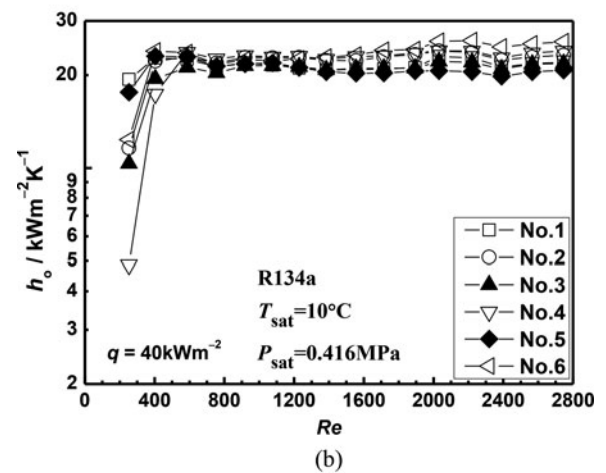
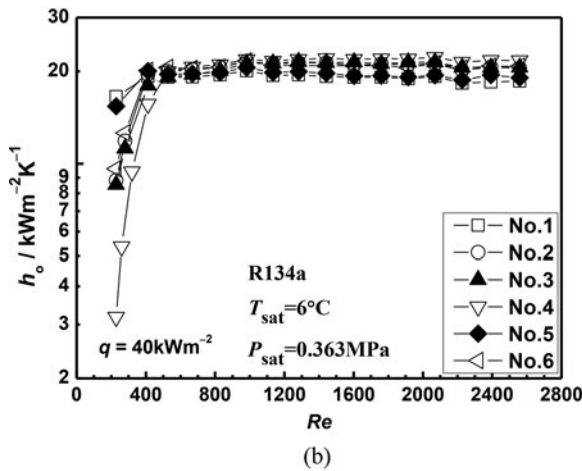
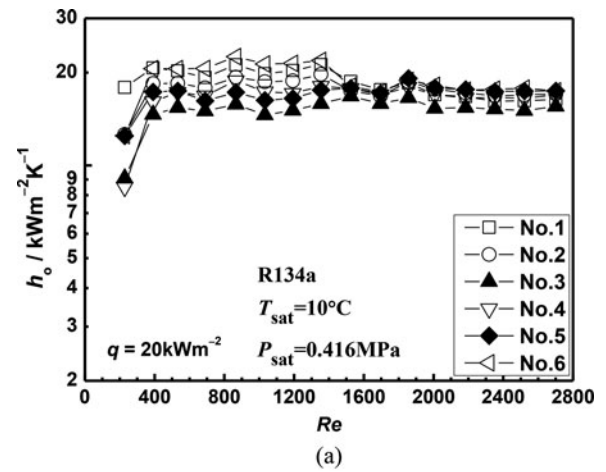
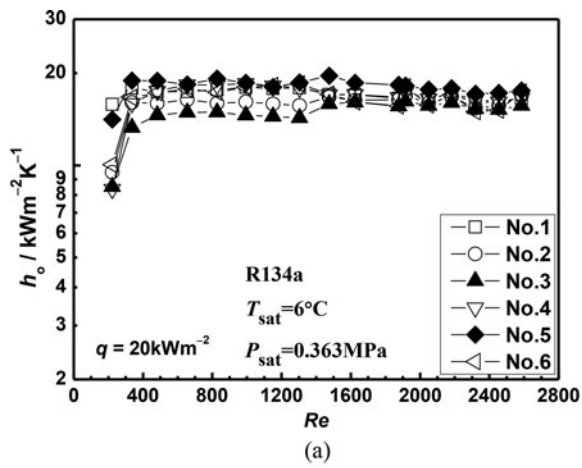


Figure 5. Local heat transfer coefficients on each individual tube at different heat fluxes of 20, 40, and 60 kWm^{-2} and saturation temperature of 6°C.

Figure 6. Local heat transfer coefficients on each individual tube at different heat fluxes of 20, 40, and 60 kWm^{-2} and saturation temperature of 10°C.

(3) The phenomenon that the tubes at different positions exhibits different heat transfer performances is called bundle effect [16]. Tube bundle effect is primarily caused by the uneven liquid distribution among tubes at different vertical rows. Ji et al. [16] found obvious bundle effect in the vertical bundle

with six tubes. While the present bundle effect is insignificant, because the present bundle depth (3 rows) is small, in which the liquid hunger on the lower tubes is not that serious.

(4) The bundle effect is dominated by the film flow rate and heat flux to a great extent. At smaller

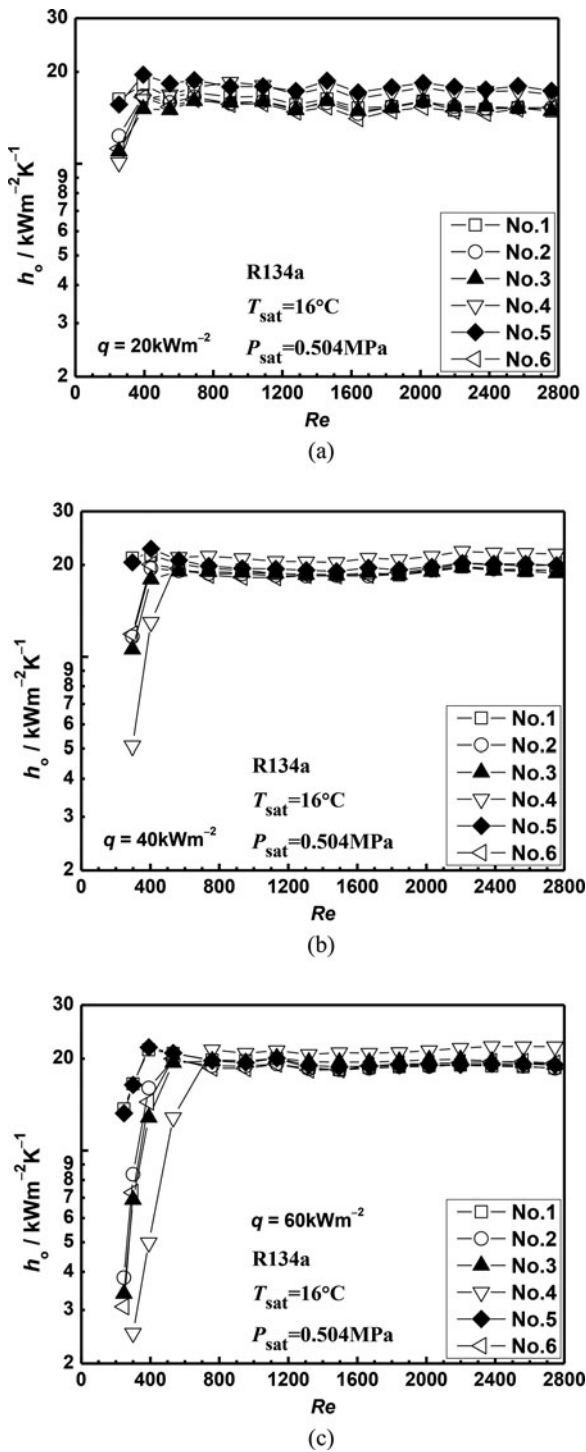


Figure 7. Local heat transfer coefficients on each individual tube at different heat fluxes of 20, 40, and 60 kWm^{-2} and saturation temperature of 16°C.

film flow rate, the significant bundle effects are observed. And also, the bundle effect becomes more obvious with increase of heat flux. However, the bundle effect becomes insignificant with increase of saturation temperature due to decrease of liquid viscosity.

- (5) With increase of saturation temperature, the heat transfer coefficient of each individual tube apparently increases from 6 to 10°C, while slightly declines from 10 to 16°C.
- (6) For three saturation temperatures, with increase of heat flux the heat transfer coefficient dramatically increases from 20 to 40 kWm^{-2} , while almost remains the same from 40 to 60 kWm^{-2} .

Falling film heat transfer results with extra cross vapor stream effect

Experiments with extra cross vapor stream effects are performed at the vapor velocity of 0 – 2.4 ms^{-1} . Here, the vapor velocity is the one at the smallest clearance of the tubes, viz. the net spacing of 3.25 mm.

Figure 8 shows the falling film evaporation heat transfer coefficients of each individual tube versus vapor velocity at different film flow rates and heat fluxes, from which the following features can be noted:

- (1) The extra vapor stream has complicated influence on the falling film evaporation heat transfer with variations of the tube position, film flow rate, heat flux and vapor velocity. These factors influence the local vapor velocity and effective film flow rate of each tube. For all cases, the practical effects of vapor stream are strongly dependent on the area of the vapor passage, which is related to the combination of film flow rate and heat flux. For the case with smaller film flow rate, on one hand the film is vulnerable to the vapor shearing due to the smaller film thickness, while on the other hand the flow resistance of the vapor is also smaller owing to the little amount of intertubular liquid. The former may induce film breakout, while the latter may weaken the effect of vapor shearing. For the case with larger film flow rate, the opposite mechanisms in two aspects are reasonable. Besides, the resultant effects of vapor stream are close to the heat flux and film flow rate. The results shown in Figure 8 are the overcome of the two aspects.
- (2) For all cases, the bundle effect becomes more obvious with increase of vapor velocity, namely, the increasing in vapor velocity magnifies the different performances among tubes. Besides, the heat transfer coefficients of the lower tubes fluctuate more severely, which implies that these tubes are subjected stronger impact of the vapor stream. For the current test range, the tube No. 3 exhibits the lowest heat transfer coefficient in entire vapor velocity.
- (3) With increase of vapor velocity, all heat transfer coefficients show a general trend of first increase

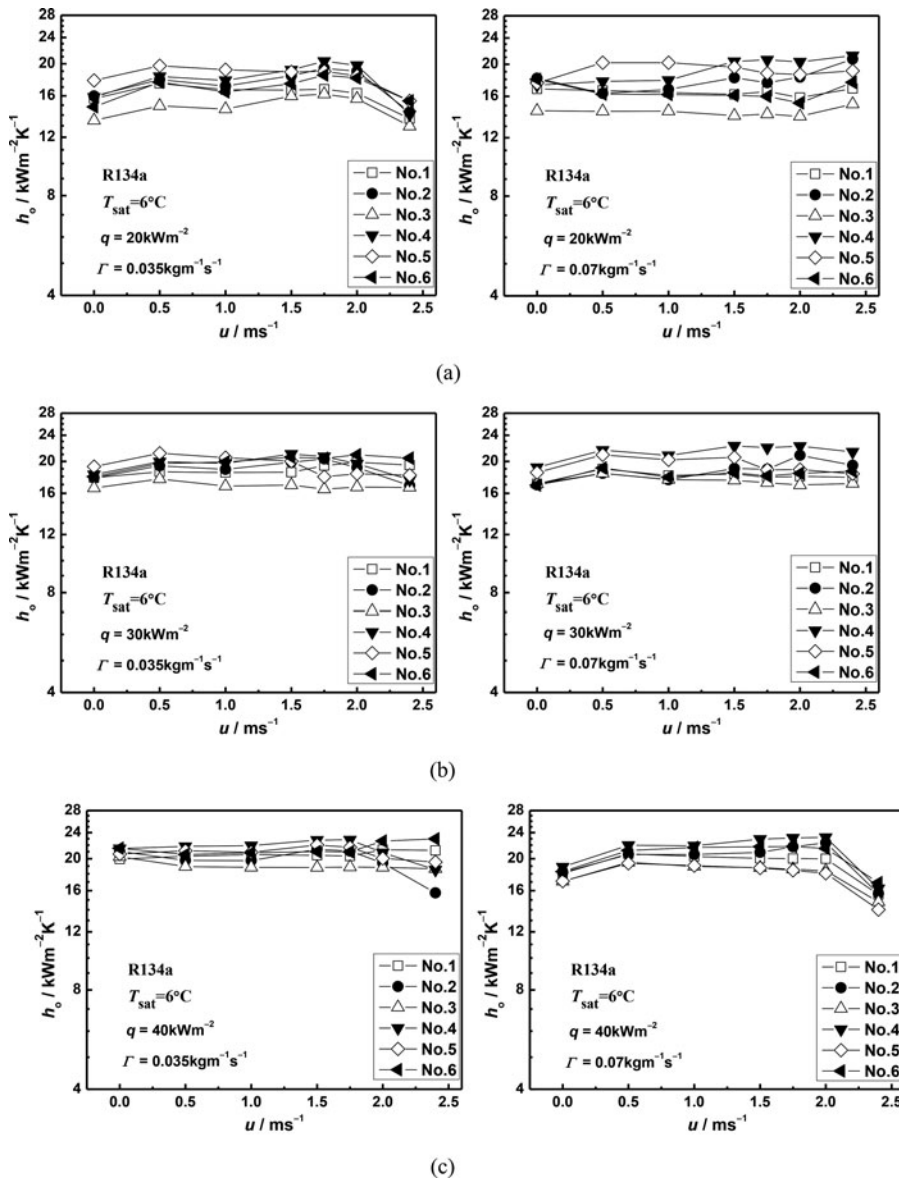


Figure 8. Falling film heat transfer coefficient versus the vapor velocity at $T_{\text{sat}} = 6^\circ\text{C}$ for $\Gamma = 0.035 \text{ kg m}^{-2} \text{ s}^{-1}$ (left) and $\Gamma = 0.07 \text{ kg m}^{-2} \text{ s}^{-1}$ (right): (a) $q = 20 \text{ kW m}^{-2}$, (b) $q = 30 \text{ kW m}^{-2}$ and (c) $q = 40 \text{ kW m}^{-2}$.

then decrease. According to these variation trends, we can see both positive and negative effects of cross vapor stream on falling film heat transfer. The positive effect may be attributed to four mechanisms: the film thickness reduction by the vapor stripping; more uniform of film distribution due to redistribution and liquid film disturbance by the vapor shearing; and reduction of velocity wake region near the lower stagnation point. While with further increase of the vapor velocity, the heat transfer coefficients decrease to the smallest levels. The negative effect is related to the liquid entrainment or film deflection even dryout at the upwind regions caused by the excessive vapor shearing.

- (4) For a given film flow rate, with increase of heat flux the falling film heat transfer coefficient increases obviously, which is similar to the behavior in the cases without the extra cross vapor. Besides, the increasing of heat flux reduces the scattering of the heat transfer coefficients. Take the cases with the smaller film flow rate for instance, with heat flux increases from 20 to 40 kW m^{-2} the heat transfer coefficients of all tubes range from 12 to 20 $\text{kW m}^{-2} \text{ K}$ at 20 kW m^{-2} , from 16.5 to 21 $\text{kW m}^{-2} \text{ K}$ at 30 kW m^{-2} and from 17.5 to 22 $\text{kW m}^{-2} \text{ K}$ at 40 kW m^{-2} .
- (5) Compared with the smaller film flow rate, the larger film flow provides higher heat transfer coefficients. This is reasonable, larger film flow rate

means higher endurance of the film to the vapor shearing.

- (6) It seems that the heat transfer coefficients fluctuate stronger with vapor velocity for the case with smaller film flow rate at the lowest heat flux (20 kWm^{-2} and $0.035 \text{ kgm}^{-1}\text{s}^{-1}$), or the one with larger film flow rate at the highest heat flux (40 kWm^{-2} and $0.07 \text{ kgm}^{-1}\text{s}^{-1}$).

Vapor stream influencing factor of the tube bundle

In this section, the bundle average heat transfer coefficient is proposed to evaluate the global effect of cross vapor stream on the tube bundle, which is given by:

$$h_{o\text{-ave}} = Q/[A_{\text{total}}(T_{w,\text{ave}} - T_{\text{sat}})] \quad (12)$$

where, for all test tubes, $Q = \Sigma Q_m$, is the total heat transfer rate, $A_{\text{total}} = \Sigma A_{o,m}$, is the total surface area for heat transfer, $T_{w,\text{ave}}$ is the mean wall temperature.

Figure 9 displays the relationship of the average falling film heat transfer coefficient versus the vapor velocity. As shown, with increase of vapor velocity, the average heat transfer coefficients first increase and then decrease. The turning point at which the trend transits from increase to decrease varies with heat flux and film flow rate. Besides, it can also be observed that the vapor flow promotes overall heat transfer when $u < 2.0 \text{ ms}^{-1}$, while prohibits overall heat transfer when $u > 2.0 \text{ ms}^{-1}$ for all cases.

Here, the ratio of $h_{o\text{-ave}}$ to the one without vapor effect is defined to reflect the effect of cross vapor stream, which is defined as vapor stream influencing factor: $K_{\text{ave}} = h_{o\text{-ave}}/h_{o\text{-ave-no vapor}}$. The variations of K_{ave} with increase of vapor velocity for all cases are illustrated in Figure 10. It can be seen that:

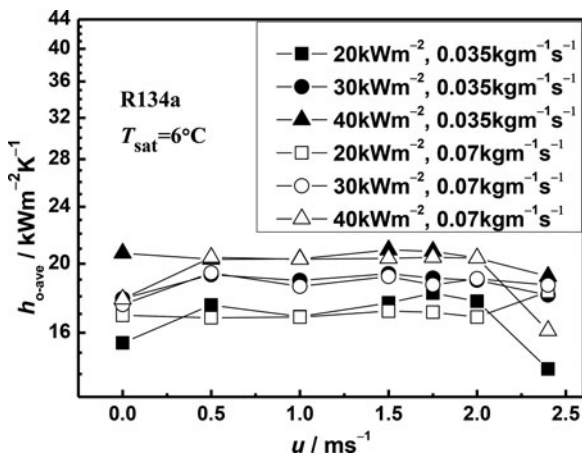


Figure 9. Average heat transfer performance of tube bundle at heat fluxes of 20, 30, and 40 kWm^{-2} and film flow rates of 0.035 and $0.07 \text{ kgm}^{-1}\text{s}^{-1}$.

- (1) The cross vapor stream has the strongest positive effect on the case with $q = 40 \text{ kWm}^{-2}$ and $\Gamma = 0.07 \text{ kgm}^{-1}\text{s}^{-1}$ and the one with $q = 20 \text{ kWm}^{-2}$ and $\Gamma = 0.035 \text{ kgm}^{-1}\text{s}^{-1}$. For the current test section and test range, the K_{ave} varies from 0.9 to 1.17.
- (2) The cross vapor stream is beneficial to the heat transfer in all cases except two extreme ones with $q = 20 \text{ kWm}^{-2}$, $\Gamma = 0.07 \text{ kgm}^{-1}\text{s}^{-1}$ and $q = 40 \text{ kWm}^{-2}$, $\Gamma = 0.035 \text{ kgm}^{-1}\text{s}^{-1}$. The former case has the larger film flow rate while the lowest evaporation amount, which provides the thickest liquid film, namely the largest vapor flow resistance, and conversely, the latter case provides the smallest vapor flow resistance. For two cases, the effect of the cross vapor stream is insignificant.

Visualization

During experiments, the liquid behaviors influenced by the cross vapor stream are observed. At the conditions without extra vapor, the liquid film is symmetrically distributed outside the tubes. However, under the shearing of the cross vapor, the film is deflected away from the central line, and a lot of splashing liquid is observed from the window. Besides, the column deflection and the droplet entrainment at larger heat flux and film flow rate are more serious than lower heat flux and film flow rate.

Figure 11 shows the photographs taken with a high definition digital camera to describe the effects of the film flow rate, heat flux, and vapor velocity on the liquid film flow behaviors. From these figures we can see that:

- (1) For the cases without extra cross vapor stream the liquid flow is very calm, while once there is

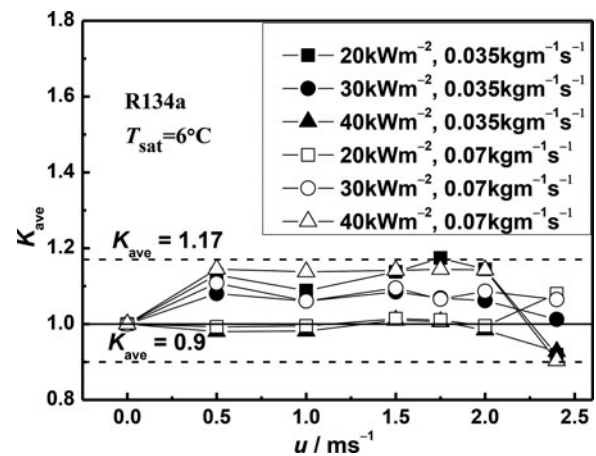


Figure 10. Cross vapor stream effect on falling film evaporation in tube bundle at heat fluxes 20, 30, and 40 kWm^{-2} and film flow rates of 0.035 and $0.07 \text{ kgm}^{-1}\text{s}^{-1}$.

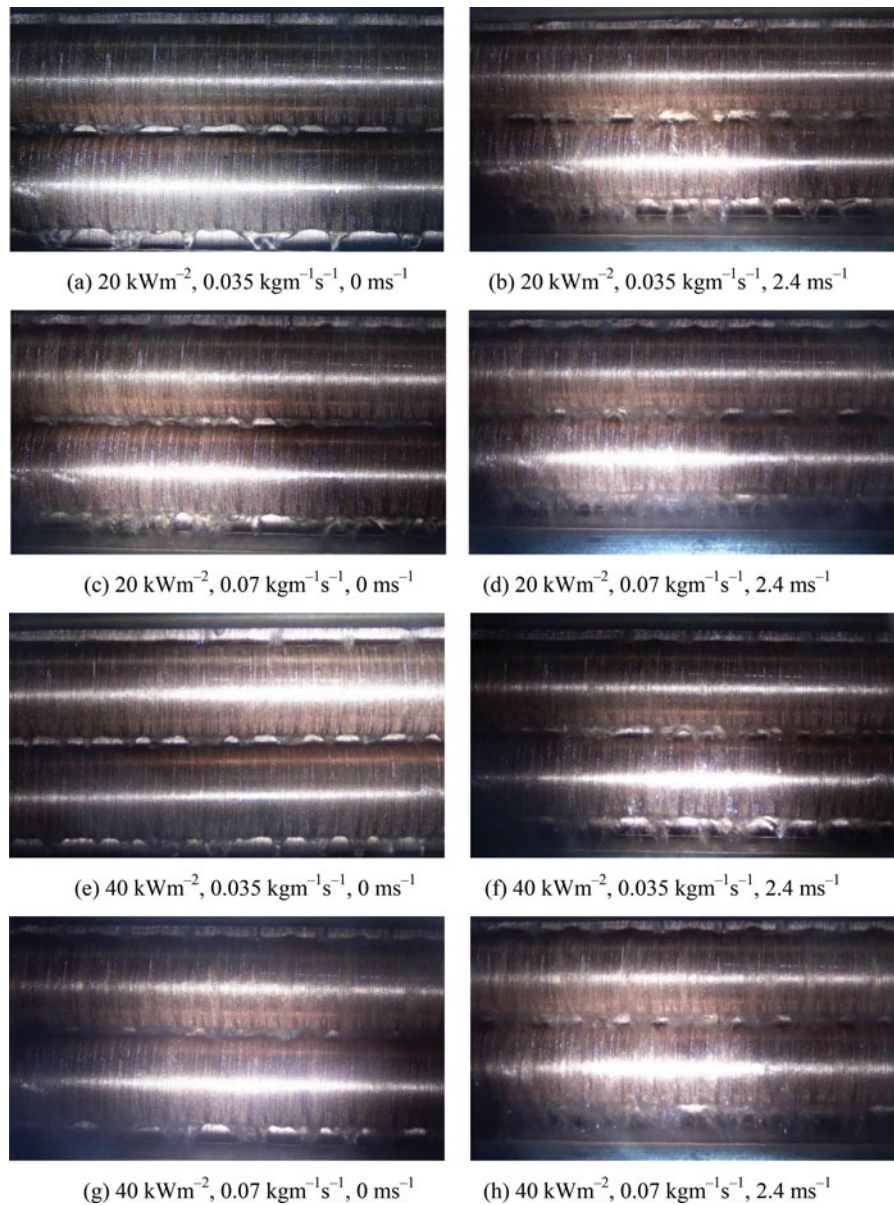


Figure 11. Liquid distribution and splash behaviors with the variation of the film flow rate, heat flux, and cross vapor velocity.

extra vapor the film flow grows turbulent, and with increase of vapor velocity the liquid amount on the outer most column (tubes No. 5 and 6) increases.

- (2) In this test, the film flow rate on the outer most column tubes increases with increase of vapor velocity. With increase of vapor velocity, the inter-tubular flow pattern on the outer most column changes from column to column-sheet even to sheet (with increase of film flow rate, the flow pattern changes in such order: droplet, droplet-column, column, column-sheet, and sheet, and the flow pattern such as column-sheet means the one between column and sheet), the amount of liquid entrained by the vapor increases, and the

displacement of the liquid blown by the vapor increases.

- (3) The liquid amount on the outermost column tubes increases obviously at the higher heat flux compared with the lower one, which is because there generates more vapor during evaporation at higher heat flux.

Conclusions

In this paper, the characteristics of falling film evaporation with nucleate boiling on a horizontal tube bundle are experimentally investigated, and the effects of cross vapor stream on heat transfer in a specially designed test section

are described. Based on the results, the following conclusions can be drawn:

- (1) With decrease of film flow rate the heat transfer coefficient of each individual tube presents two clear stages: first remains constant and then drops rapidly. The transition film flow rate varies with tube positions and heat fluxes.
- (2) Under the current test range, with increase of saturation temperature the heat transfer performance is firstly promoted and then inhibited.
- (3) The cross vapor stream has complicated influence on the falling film evaporation depending on the tube position, film flow rate, heat flux and vapor velocity. With increase of cross vapor velocity, the heat transfer coefficients for all cases show the general trend of first increase then decrease.
- (4) The cross vapor generally has more remarkable enhancement effects on heat transfer at larger film flow rate or at the lower heat flux.

Nomenclature

A	Area, m^2
c_i	Enhancement factor of internal tube wall
c_p	Specific heat capacity, $Jkg^{-1}K^{-1}$
d	Droplet diameter, m
d_p	Largest droplet diameter, m
d^*	Effective diameter of the liquid column in Eq. (3)
D	Diameter of tube, m
g	Gravity acceleration, ms^{-2}
h	Heat transfer coefficient, $Wm^{-2}K^{-1}$
h_{gni}	Heat transfer coefficient calculated by the Gnielinski equations [23], $Wm^{-2}K^{-1}$
H	Tube pitch, m
k	Overall heat transfer coefficient, $Wm^{-2}K^{-1}$
K	Ratio of heat transfer coefficient
L	Tested length of tube, m
\dot{m}	Mass flow rate, kgs^{-1}
\dot{m}_g	Mass flow rate of the extra vapor, kgs^{-1}
n	Coefficient in definition of λ in Eq. (3)
P	Power, W
q	Heat flux, Wm^{-2}
Q	Total heat transfer rate of the tube bundle, W
R	Thermal resistance, m^2KW^{-1}
r	Latent heat, Jkg^{-1}
Re	Film Reynolds number
S	Net tube spacing in Eq. (3)
T	Temperature, K
u	Velocity, ms^{-1}

Greek symbols

Δ	Variable differential
Γ	Liquid film flow rate on one side of the tube per unit length, $kgm^{-1}s^{-1}$
Φ	Heat transfer rate, W
θ	Critical deflection angle of the liquid column in Eq. (3), degree
λ	Thermal conductivity, $Wm^{-1}K^{-1}$
μ	Dynamic viscosity, $kgm^{-1}s^{-1}$
ρ	Density, kgm^{-3}
σ	Surface tension, Nm^{-1}

Subscripts

ave	Average variable
c	Condensing
e	Evaporating
f	fouling
G	Gas refrigerant
L	Liquid refrigerant
LMTD	Logarithmic mean temperature difference
m	Number of evaporating tube in Eq. (5)
n	Number of condensing tube in Eq. (6)
i	Inside of tube
o	Outside of tube
p	Refrigerant pump
sat	Saturation
w	Wall

Acknowledgment

The supports from the National Key Basic Research Program of China (973 Program) (2013CB228304), Research Fund for the Doctoral Program of Higher Education of China(20120201130007), NSFC(51306140), and Daikin Cooperation of Japan are greatly acknowledged.

Notes on contributors



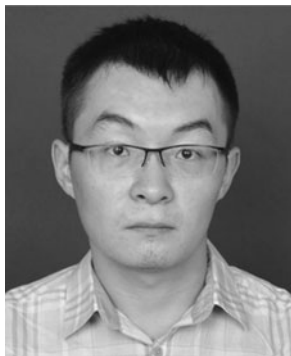
Chuang-Yao Zhao is a Ph.D. student in the School of Energy and Power Engineering at Xi'an Jiaotong University, China, under the supervision of Prof. Wen-Quan Tao. He obtained his master's degree in 2007 from the Lanzhou Jiaotong University, where he studied the numerical simulation on the fluid flow and heat transfer using body fitted based finite volume method. His main interests are enhanced heat transfer technology in refrigeration and air conditioning. He

is also interested in the numerical simulation on the problems with free surface flow or phase change heat transfer in micro/mini channel.



Wen-Tao Ji received his Ph.D. with Prof. Wen-Quan Tao from Xi'an Jiaotong University in 2012. He was a visiting scholar at Air Conditioning and Refrigeration Center in the Department of Mechanical Science and Engineering at University of Illinois at Urbana-Champaign in 2014-2015. He is now an associate professor in Key Laboratory of Thermo-Fluid Science and Engineering of MOE at XJTU,

China. His research has been focused on two-phase heat transfer, falling film evaporation, supercritical CO₂, compact heat exchangers. He has 10 first-author archival papers.



Pu-Hang Jin is a Ph.D. student in the School of Energy and Power Engineering at Xi'an Jiaotong University, China. He was a visiting student and enrolled in two graduate courses at University of California, Riverside for half a year in 2014. He also obtained his bachelor's degree in 2014 in the same institute. His research is focused on the phase change especially boiling mechanisms both by

experimental and simulation methods.



Wen-Quan Tao is a professor of engineering thermophysics at Xi'an Jiaotong University, Xi'an, China. He graduated from Xi'an Jiaotong University in 1962 and received his graduate diploma in 1966. He has published more than 400 journal articles and international conference papers in the areas of engineering thermophysics. He is also the author or co-author of nine textbooks.

His recent research interests include advanced numerical methods in fluid flow and heat transfer, enhancement of heat transfer, heat transfer in micro and nano configurations, application of renewable energy, and energy efficiency evaluation.

References

- [1] Ribatski, G., and Jacobi, A. M., Falling-Film Evaporation on Horizontal Tubes—a Critical Review, *International Journal of Refrigeration*, vol. 28, no. 5, pp. 635–653, 2005.
- [2] Fernández-Seara, J., and Pardiñas, Á. Á., Refrigerant Falling Film Evaporation Review: Description, Fluid Dynamics and Heat Transfer, *Applied Thermal Engineering*, vol. 64, no. 1–2, pp. 155–171, 2014.
- [3] Abed, A. M., Alghoul, M. A., Yazdi, M. H., Al-Shamani, A. N., and Sopian, K., The Role of Enhancement Techniques on Heat and Mass Transfer Characteristics of Shell and Tube Spray Evaporator: A Detailed Review, *Applied Thermal Engineering*, vol. 75, pp. 923–940, 2015.
- [4] Liu, Z. H., and Ishibashi, E., Enhanced Boiling Heat Transfer of Water/Salt Mixtures in the Restricted Space of the Compact Tube Bundle, *Heat Transfer Engineering*, vol. 22, no. 3, pp. 4–10, 2001.
- [5] Bogan, N., and Park, C., Influences of Solution Subcooling, Wall Superheat and Porous-Layer Coating on Heat Transfer in a Horizontal-Tube, Falling-Film Heat Exchanger, *International Journal of Heat And Mass Transfer*, vol. 68, no. 1, pp. 141–150, 2014.
- [6] He, Y. Q., Bi, Q. C., Zhang, J. C., and Hou, H., Experimental Study on the Heat Transfer Characteristics of an Evaporating Falling Film on a Horizontal Plain Tube, *Heat Transfer Engineering*, vol. 32, no. 11-12, pp. 936–942, 2011.
- [7] Roques, J. F., and Thome, J. R., Falling Films on Arrays of Horizontal Tubes with R-134a, Part I: Boiling Heat Transfer Results for Four Types of Tubes, *Heat Transfer Engineering*, vol. 28, no. 5, pp. 398–414, 2007.
- [8] Roques, J. F., and Thome, J. R., Falling Films on Arrays of Horizontal Tubes with R-134a, Part II: Flow Visualization, Onset of Dryout, and Heat Transfer Predictions, *Heat Transfer Engineering*, vol. 28, no. 5, pp. 415–434, 2007.
- [9] Chang, T. B., Li, J. C., and Liang, C. C., Heat Transfer Enhancement of Square-Pitch Shell-and-Tube Spray Evaporator Using Interior Spray Nozzles, *Heat Transfer Engineering*, vol. 32, no. 1, pp. 14–19, 2011.
- [10] Parken, J. W. H., Heat Transfer to Thin Water Films on Horizontal Tubes, Ph.D. Thesis, The State University of New Jersey, New Brunswick, 1975.
- [11] Armbruster, R., and Mitrovic, J., Heat Transfer in Falling Film on a Horizontal Tube, Proceedings of the national heat transfer conference, Portland, [ASME HTD-vol. 314], vol. 12, pp. 13–21, 1995.
- [12] Hu, X., The Intertube Falling-Film Modes: Transition, Hysteresis, and Effects on Heat Transfer, Ph.D. Thesis, University of Illinois, Urbana-Champaign, 1995.
- [13] Tatara, R. A., and Payvar, P., Measurement of Spray Boiling Refrigerant Coefficients in an Integral-Fin Tube Bundle Segment Simulating a Full Bundle, *International Journal of Refrigeration*, vol. 24, no. 8, pp. 744–754, 2001.
- [14] Liu, P. J. P., The Evaporating Falling Film on Horizontal Tubes, Ph.D. Thesis, University of Wisconsin, Madison, 1975.
- [15] Ribatski, G., and Thome, J. R., A Visual Study of R134a Falling Film Evaporation on Enhanced and Plain Tubes, 5th International Symposium, Heat Mass Transfer and Energy Conversion, Xi'an, China, July 3-6, 2005.
- [16] Ji, W. T., Zhao, C. Y., He, Y. L., Xi, G. N., and Tao, W. Q., Vapor Flow Effect on Falling Film Evaporation of R134a Outside Horizontal Tube Bundle, The 15th International Heat Transfer Conference, Kyoto, Japan, August 10-15, 2014.
- [17] Danilova, G. N., Burkin, V. G., and Dyundin, V. A., Heat Transfer in Spray-Type Refrigerator Evaporators,

- Heat Transfer-Soviet Research*, vol. 8, no. 6, pp. 105–113, 1976.
- [18] Ruan, B., Jacobi, A. M., and Li, L., Effects of a Countercurrent Gas Flow on Falling-Film Mode Transitions between Horizontal Tubes, *Experimental Thermal And Fluid Science*, vol. 33, no. 8, pp. 1216–1225, 2009.
- [19] Yung, D., Lorenz, J. J., and Ganic, E. N., Vapor/Liquid Interaction and Entrainment in Falling Film Evaporators, *ASME Journal of Heat Transfer*, vol. 102, no. 1, pp. 20–25, 1980.
- [20] Lemmon, E. W., Huber, M. L., and McLinden, M. O., *Reference Fluid Thermodynamic and Transport Properties (Refprop), Version 8.0*, in, National Institute of Standards and Technology (NIST), Gaithersburg, Maryland, USA, 2008.
- [21] Yang, S. M., and TAO, W. Q., *Heat Transfer*, Higher Education Press, Beijing, 2006.
- [22] Zhao, C. Y., Jin, P. H., Ji, W. T., and Tao, W. Q., Heat Transfer Correlation of the Falling Film Evaporation on a Single Horizontal Smooth Tube, *Applied Thermal Engineering*, vol. 103, pp. 177–186, 2016.
- [23] Gnielinski, V., New Equations for Heat and Mass Transfer in the Turbulent Flow in Pipes and Channels, *International Chemical Engineering*, vol. 16, no. 2, pp. 359–368, 1976.
- [24] Cheng, B., and Tao, W. Q., Experimental Study of R-152a Film Condensation on Single Horizontal Smooth Tube and Enhanced Tubes, *ASME Journal of Heat Transfer*, vol. 116, no. 1, pp. 266–270, 1994.
- [25] Kline, S. J., The Purposes of Uncertainty Analysis, *ASME Journal of Fluids Engineering*, vol. 107, no. 2, pp. 153–160, 1985.
- [26] Nusselt, W., Die Oberflächencondensation Des Wasserdampfes, *VDI*, vol. 60, no. 27–28, pp. 541–569, 1916.